CrossMark

Electronic Transport and Raman Spectroscopy Characterization in Ion-Implanted Highly Oriented Pyrolytic Graphite

R. F. de Jesus[1] · A. M. Turatti[1,3] · B. C. Camargo[2,4] ·
R. R. da Silva[2] · Y. Kopelevich[2] · M. Behar[1] · N. M. Balzaretti[1] ·
M. A. Gusmão[1] · P. Pureur[1]

Abstract We report on Raman spectroscopy, temperature-dependent in-plane resistivity, and in-plane magnetoresistance experiments in highly oriented pyrolytic graphite (HOPG) implanted with As and Mn. A pristine sample was also studied for comparison. Two different fluences were applied, $\varphi = 0.5 \times 10^{16}$ ions/cm^2 and $\varphi = 1.0 \times 10^{16}$ ions/cm^2. The implantations were carried out with 20 keV ion energy at room temperature. The Raman spectroscopy results reveal the occurrence of drastic changes of the HOPG surface as a consequence of the damage caused by ionic implantation. For the higher dose, the complete amorphization limit is attained. The resistivity and magnetoresistance results were obtained placing electrical contacts on the irradiated sample surface. Owing to the strong anisotropy of HOPG, the electrical current propagates mostly near the implanted surface. Shubnikov–de Haas (SdH) oscillations were observed in the magnetoresistance at low temperatures. These results allow the extraction of the fundamental SdH frequencies and the carriers' effective masses. In general, the resistivity and magnetoresistance results are consistent with those obtained from Raman measurements. However, one must consider that the electrical conduction in our samples occurs as in a parallel association of a largely resistive thin sheet at the surface strongly modified by disorder with a thicker layer where damage produced by

---

✉ P. Pureur
ppureur@if.ufrgs.br

1 Instituto de Física, Universidade Federal do Rio Grande do Sul, Porto Alegre, RS 91501-970, Brazil

2 Instituto de Física "Gleb Wathagin", Universidade Estadual de Campinas, UNICAMP, Campinas, SP 13083-970, Brazil

3 Instituto de Matemática, Estatística e Física, Universidade Federal do Rio Grande, FURG, Rio Grande, RS 93206-900, Brazil

4 Institute of Physics, Polish Academy of Sciences, Aleja Lonikow 32/46, 02-668 Warsaw, Poland

implantation is less severe. The SdH oscillations do not hint to significant changes in the carrier density of HOPG.

Keywords Graphite · Ion implantation · Raman scattering · Magnetoresistance · SdH oscillations

1 Introduction

The physical properties of graphite have been extensively re-examined in the light of the recent and intense investigations devoted to the understanding of graphene [1]. Both the properties of the single layer graphene and those of systems formed by few atomic graphene layers [2] have been invoked to explain the physics of graphite. Some authors suggest that graphite may be regarded as a simple stack of graphene planes [3]. However, several physical properties of this 3D-carbon system have been shown to be crucially dependent on the conditions of sample preparation. With this regard, synthetic graphite samples grown at elevated temperatures and high pressures, known as highly pyrolytic oriented graphite (HOPG), are particularly interesting because of their strong texture characterized by a rather good c-axis alignment of platelet-like crystallites [4]. The thermodynamic stable intercalation form of the graphene planes in graphite is the ABA stacking, well known as the Bernal sequence [5], characterized by $D_{6H}^4 - P6_3/mmc$ space group, containing four atoms per unit cell [6].

The electronic band structure for ideal ABA stacking graphite was first studied by Wallace who showed that a single graphene layer is a zerogap semiconductor [7]. Later on, Slonczewski and Weiss (SW) proposed a phenomenological model taking into account the intralayer C–C coupling [8]. These authors conclude that graphite is a semimetal with a small band overlap close to the H–K–H vertices of the first Brillouin zone. McClure [9] demonstrated that the intralayer C–C overlap is about 0.03 eV and the Fermi surface for majority carriers is formed by two hole-type and one electron-type elongated pockets placed along the H–K–H edge.

The weak interlayer interaction and the high alignment along c-axis make the HOPG samples highly anisotropic systems, showing good electrical and thermal in-plane conduction [6]. On the other hand, due to the smallness of the Fermi surface pockets, the small hole and electron effective masses and the generally good sample quality, the HOPG specimens usually reach the quantization condition ($\omega_c \tau \gg 1$, where ω_c is the cyclotron frequency and τ is the relaxation time for in-plane transport) at moderate magnetic fields applied parallel to the c-axis. Consequently, Shubnikov–de Haas (SdH) and de Haas–van Alphen oscillations are commonly observed in electrical transport [10,11] and magnetization [12,13] measurements, respectively.

Several studies have been done on natural and synthetic graphite submitted to ion implantation [14–18] since this technique leads to relevant modifications in the physical and chemical properties of materials' surface by producing strong disorder at the microscopic level as much as by introducing impurities at precisely controlled concentrations [19]. Most of the investigations on ion-implanted graphite are related to magnetic [15–18] or electrical transport [18,19] properties of HOPG. Irradiation with protons [20,21] or neutrons [22] was also intensively employed to study the role of defects on the magnetic properties of graphite.

Raman spectroscopy has been intensively employed to characterize carbon-based materials [23]. Systems such as diamond [24–26], graphene (monolayer, bilayer and trilayer) [27,28] and graphite [26,28–30] have been experimentally and theoretically studied. Effects of ion irradiation in graphite have also been addressed with basis on Raman scattering results [29,31–33].

In this work, we have carried out Raman spectroscopy and electrical transport experiments in HOPG samples implanted with Mn and As. The manganese is expected to play as a magnetic impurity, whereas the arsenide might produce electron doping in graphite. The implantations were performed at 20 keV with fluences $\varphi = 0.5 \times 10^{16}$ ions/cm^2 and $\varphi = 1.0 \times 10^{16}$ ions/cm^2. A pristine HOPG specimen was also studied as a reference sample. The Raman spectra showed that the graphite surface becomes amorphous when submitted to fluences of the order 10^{16} ions/cm^2. The planar magnetoresistance (MR) amplitude at fixed field and temperature varies significantly with the fluence and the implanted ion. However, for both Mn and As, the MR amplitude goes through a maximum at $\varphi = 0.5 \times 10^{16}$ ions/cm^2 and decreases for higher fluences, as previously observed in other implanted HOPG samples [18,19]. Quantum oscillations are observed in the MR, so that the fundamental frequencies and the cyclotron effective masses could be estimated from the Lifshitz–Kosevich (LK) theory [34]. We conclude that the obtained Raman and MR results are strongly influenced by the damage produced by the ion implantation process.

2 Experimental

2.1 Sample Preparation and Characterizations

A pristine sample of SPI-I graphite furnished by SPi Supplies$^@$ with $5 \times 5 \times 1$ mm dimension was characterized by means of X-ray diffraction using Cu Kα radiation. Figure 1 shows the X-ray spectrum obtained when diffraction is due to the graphene planes. Only the (002), (004) and (006) lines could be observed. The angular positions of these peaks are within the values reported in the literature for HOPG [35]. The inset in Fig. 1 shows the rocking curve obtained from the (002) line (angular position $2\theta \sim 26°$). The full-width at half-maximum (FWHM $\sim 1.02°$) was extracted from a Gaussian fitting profile. This value reveals that our HOPG sample is characterized by a relatively high value for mosaicity [36]. Several thin samples were carefully exfoliated from this original monolith by using adhesive tape. These samples have the form of irregular platelets with thickness around 6 μm and average lateral size of 3 mm. Four of these new specimens were then irradiated with one of the two ions, Mn$^+$ and As$^+$, with 20 keV energy at room temperature. Two different doses, $\varphi = 0.5 \times 10^{16}$ ions/cm^2 and $\varphi = 1.0 \times 10^{16}$ ions/cm^2, were implanted for each ion. No annealing was made after implantation in order to preserve the quenched disorder produced by ion irradiation. The distribution of the implanted ions has an approximately Gaussian profile, as determined by simulations based on the software SRIM [37]. The implantations were carried out with the 500 kV Ion Implanter of the Instituto de Física, UFRGS. The relevant parameters for the implantation processes are listed in Table 1. Several of the exfoliated samples were not implanted. Four of

Fig. 1 X-ray diffraction pattern for SPI-I HOPG. The inset shows the rocking curve corresponding to the (002) line. Line intensities are given in arbitrary units (a.u.)
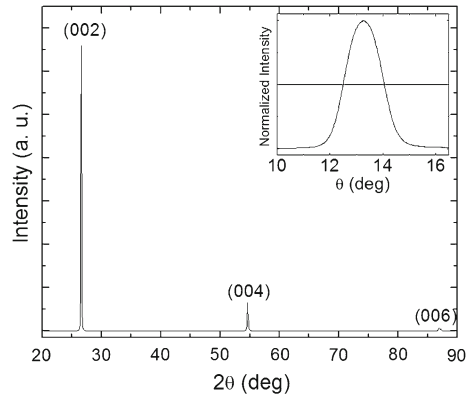

Table 1 Parameters of the implantation processes in SPI-I HOPG

Parameters	Sample			
Ion	As		Mn	
Current (nA)	150	150	150	150
Energy (keV)	20	20	20	20
Fluence[a] (10^{16}cm^{-2})	0.5	1.0	0.5	1.0
Temperature (°C)	30	30	30	30
Depth[b] (nm)	16.4	16.4	18.0	18.0
Straggling (nm)	3.6	3.6	4.4	4.4
Concentration (%)	5	10	3.8	7.4
Sample label	As(0.5)	As(1.0)	Mn(0.5)	Mn(1.0)

[a] Nominal fluence, as irradiated
[b] Maximum of the Gaussian profile

them were selected for use as reference specimens in the Raman experiments. One of these pure samples was also studied for its electrical transport properties.

2.2 Raman Spectroscopy

The Raman spectra for the SPI-I graphite samples were obtained at room temperature and ambient pressure using a home-assembled micro-Raman apparatus equipped with a He–Ne laser. A Super Notch Plus filter was used to eliminate Rayleigh scattering. The signal is analyzed by means of a Jobin Yvon spectrometer iHR320 model connected to a CCD detector cooled with liquid nitrogen. A He–Ne laser with 632.8 nm wavelength (red) and 10 mW incident power is focused through a 50× objective lens. The spot diameter is about 2–3 μm.

2.3 Resistance and Magnetoresistance Measurements

The electrical transport properties were measured with a Quantum Design PPMS$^{@}$ system. The electric resistance experiments were carried out in the temperature interval 2–250 K. The magnetoresistance was measured with at fixed temperatures $T = 2, 3, 5, 7$ and 10 K as a function of the magnetic field in the range $-4T \leq B \leq 4T$. The electrical measurements were made in a four-contact geometry using a DC technique with 1 mA current. Gold wires were attached with silver paste to four contacts previously deposited on one of the large sample surfaces. Special care was taken with respect to the configuration for the electrical contacts placed on the investigated samples. The pairs of current and voltage leads were deposited exclusively on the irradiated surface of each sample, as depicted in the inset of Fig. 4. Owing to the large planar anisotropy of HOPG, this contact configuration assures that a significant fraction of current probes the superficial region of the samples including the thin sheet that is modified by implantation [17, 18]. Based on the anisotropy of the HOPG conductivity and in the geometrical configuration of the electrical contacts, we estimate that a large fraction of the current circulates within a layer with thickness of the order $0.1 \, \mu$m. This estimation is also based on the results obtained by Koren et al. [38] who studied the anisotropic propagation of the electrical current injected on the graphite surface. In our experiments, the applied magnetic field was kept parallel to the c-axis ($B//c$) of the HOPG specimens, while the current flowed parallel to the graphene planes.

The planar MR is defined as $\Delta\rho/\rho_0 = (R_{xx}(B) - R_{xx}(0))/R_{xx}(0)$. The resistance is determined as $R_{xx}(B) = V_{xx}(B)/i$, where $V_{xx}(B)$ is the longitudinal voltage measured in the presence of the magnetic induction B and i is the applied current. The values so determined for R_{xx} are sample dependent. At zero field and $T = 250$ K, resistances between 0.2 and 2 Ω were measured, with average value $R_{xx}(0) \approx 1 \, \Omega$.

3 Results and Discussion

3.1 Raman Measurements

The Raman spectra of four pure SPI-I graphite samples were registered. For each of these samples, the Raman measurements were carried out by focusing the laser light on two different points of their surface. For all samples and illuminated spots, the obtained spectra do not display noticeable differences and are consistent with known results for graphite [38]. Figure 2 shows a typical result. In panel (a) one observes the G-peak around $1582 \, \text{cm}^{-1}$ that is due to the optical phonon E_{2g} at the high symmetry point Γ. Also seen is the second-order D'-peak (or 2D-peak) situated around $2690 \, \text{cm}^{-1}$ that comes from a double-resonant scattering process at the K point symmetry [38]. In panel (b) of Fig. 2 an enlarged view of the D'-peak is shown, where one observes that a lower energy shoulder accompanies this peak. The green continuous lines in Fig. 2b are Lorentzian fittings of the D'-peak centered at $2690 \, \text{cm}^{-1}$ and of the shoulder, which is centered at $2640 \, \text{cm}^{-1}$. The pink dashed line corresponds to the sum of the two individual fittings. For all obtained spectra for the pure samples, the splitting
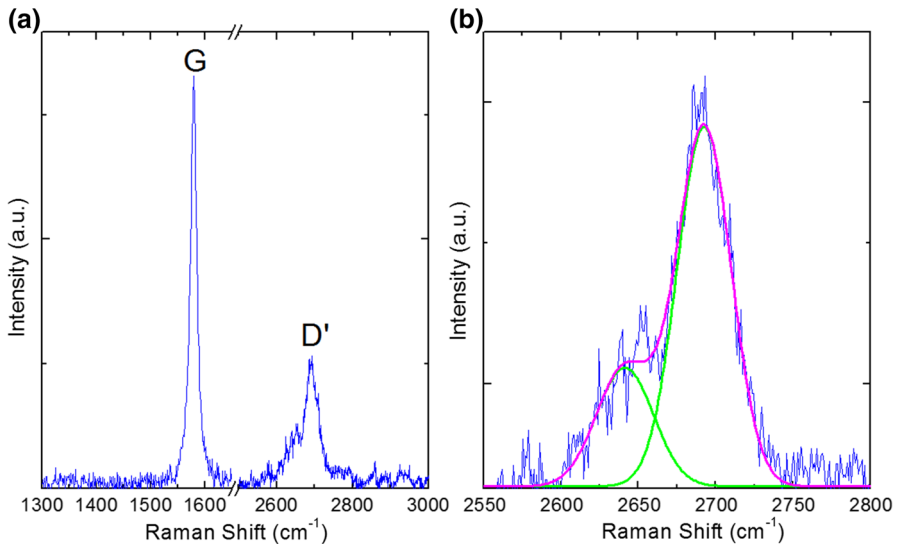
(a)

(b)

Fig. 2 Raman spectrum obtained at room temperature for a representative sample of SPI-I graphite. Identical spectra were measured in two different points of four investigated samples. Panel **a** shows the first-order line (G) located at 1580 cm^{-1} and the second-order (D') at 2690 cm^{-1}. Panel **b** shows an enlarged view of the D'-peak and its shoulder at low energies. Green continuous lines are Lorentzian fittings for the individual D'-peak and its shoulder. The pink dashed line represents the sum of the individual Lorentzians. Line intensities are given in arbitrary units (a.u.) (Color figure online)

between the main D'-line and its shoulder at lower frequency is about 50 cm^{-1}. The positions of the D'-peak and that of the accompanying shoulder agree with reported observations in Kish graphite [39] and HOPG [40]. The splitting of the D'-mode is already visible in double-layer graphene and gradually evolves to the shape displayed in Fig. 2b in films where an increasing number of graphene layers approaches that characterizing the bulk behavior [40]. One should note that the almost coinciding positions of the Raman shift in graphene and the left shoulder in the D'-line, as well as other characteristics of these lines lead authors in Ref. [41] to propose that the shoulder is reminiscent of Dirac electron transitions related to graphene monolayers present in bulk graphite. Also, noticeable in the spectrum of Fig. 2 is the absence of the so-called D-mode expected to occur at 1330 cm^{-1}, which is attributed to disorder [39]. There is no hint for the presence of the D-line in the eight Raman spectra collected from our pure SPI-I HOPG samples. This fact certifies for the good crystalline quality of the studied graphite.

Raman spectra were also obtained for SPI-I HOPG specimens implanted with Mn$^+$ and As$^+$ ions. As previously stated, the used fluences were $\varphi = 0.5 \times 10^{16}$ ions/cm^2 and $\varphi = 1.0 \times 10^{16}$ ions/cm^2. Figure 3 shows the Raman spectra obtained for the implanted samples as compared to the corresponding spectrum for the pure SPI-I graphite. For the studied ion energy, the nuclear stopping power largely dominates the propagation of ions in the crystalline matter. In these conditions, the ionic implantation usually generates considerable damage in the sample. Then, it is expected that the disorder-induced D-peak becomes observable at quite low fluences, as indeed occurs
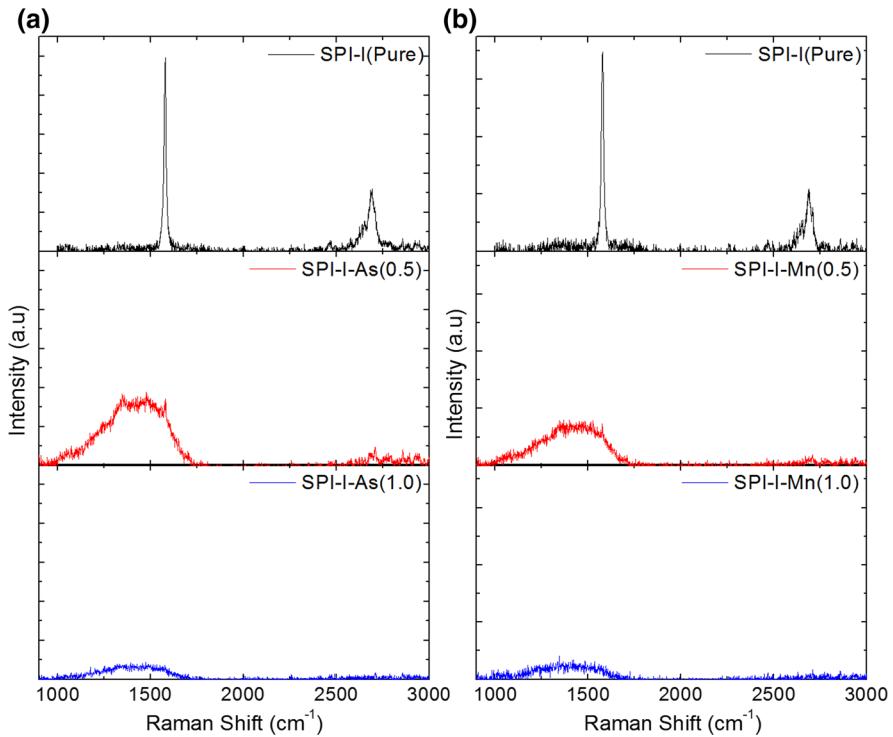
Fig. 3 Raman measurements for the samples irradiated with As, shown in the panels to the left (**a**), and Mn, shown in the panels to the right (**b**). The spectrum obtained for the pure sample is also shown for comparison. The scale for the line intensity (in arbitrary units) is the same in all spectra (Color figure online)

[31–33,42]. As the fluence increases to 10^{15} / cm^3 and above in non-annealed samples [31] the D-line starts to convolute with the G-line, and strong broadening of the first-order spectrum becomes evident. Meanwhile, the second-order D'-line also broadens and its amplitude relative to that of the pure sample decreases [31,33]. It was shown that implantation of N^+ and Ar^+ with fluence $\varphi = 1.0 \times 10^{16}$ ions/cm^2 at 20 keV energy leads to a Raman spectrum identical to that of amorphous carbon [33]. As shown in Fig. 3, the irradiation of both Mn^+ and As^+ produces a strong broadening of the first-order Raman spectrum and a progressive suppression of the second-order D'-peak. The spectra in Fig. 3 for the highest studied dose, $\varphi = 1.0 \times 10^{16}$ ions/cm^2, correspond to that observed for amorphous carbon. This observation indicates that, in this case, the damage produced by implantation led to complete destruction of the crystalline ordering near the irradiated surface of our HOPG samples.

3.2 Temperature-Dependent Resistance

Figure 4 shows the temperature-dependent electrical resistance for the pure and implanted SPI-I samples in the interval extending from $T = 2$ K up to $T = 250$ K.

Fig. 4 Normalized longitudinal resistance versus temperature for SPI-I HOPG in the pristine state and after irradiation with Mn and As in the quoted fluences. Inset shows configuration adopted for current and potential electrical contacts (Color figure online)
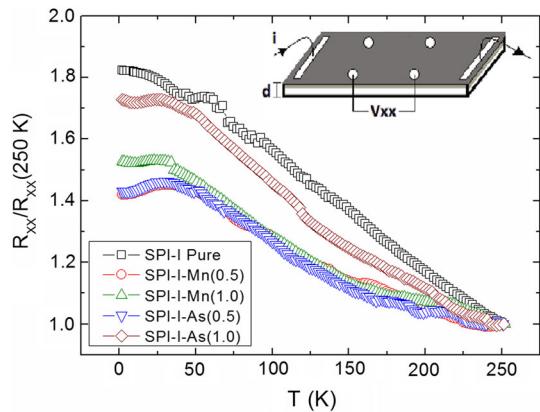
Results are normalized to $R_{xx} = 1$ in $T = 250$ K, since the inhomogeneous current distribution resulting from the adopted electrical contacts configuration makes difficult the determination of absolute values for the resistivity of the studied samples [38]. The inset of Fig. 4 shows schematically the placement of the electrical contacts on the sample surface. In all cases, $R_{xx}(T)$ is semiconductor-like. This behavior is typical of SPI-I graphite sourced by SPi Supplies[@], and it is attributed to the relatively low heat treatment temperature to which these samples are submitted during the growth process [43,44]. At low temperature, the resistances in Fig. 4 become almost temperature independent. This particularity has been attributed to the opposite temperature dependence showed by the hole mobility and the carrier density in this type of HOPG [44]. As also shown in Fig. 4, the temperature dependence of the resistance in the implanted samples is less pronounced than in the pure sample. Excepting the case of the sample irradiated with $\varphi = 1.0 \times 10^{16} \text{As/cm}^2$, the normalized resistance for the other implanted samples almost collapses into a single curve, showing that disorder is the dominant effect produced by implantation.

3.3 Magnetoresistance

Figure 5a shows the planar magnetoresistance for the pristine and irradiated samples measured at $T = 2$ K with applied fields in the interval $0 \leq B \leq 4$ T. One observes that SPI-I graphite has a giant MR when quantitatively compared to other multilayer systems. However, its magnitude is significantly smaller than that observed in some HOPG from other furnishers [18,36]. As shown in Fig. 5b, the MR amplitude in fixed field and temperature increases significantly upon implantation and goes through a maximum at $\varphi = 0.5 \times 10^{16}/\text{cm}^2$. In the higher fluence, $\Delta\rho/\rho_0$ is systematically reduced. A similar behavior of the MR was previously observed in other HOPG samples submitted to ion irradiation [17,18], independently of the implanted ion. Thus, this effect seems to be related to the disorder structure produced by irradiation rather than to electronic doping by implanted impurities. In lower fluences, single-ion vacancies are expected to be the dominant defects produced by irradiation [45]. Scattering
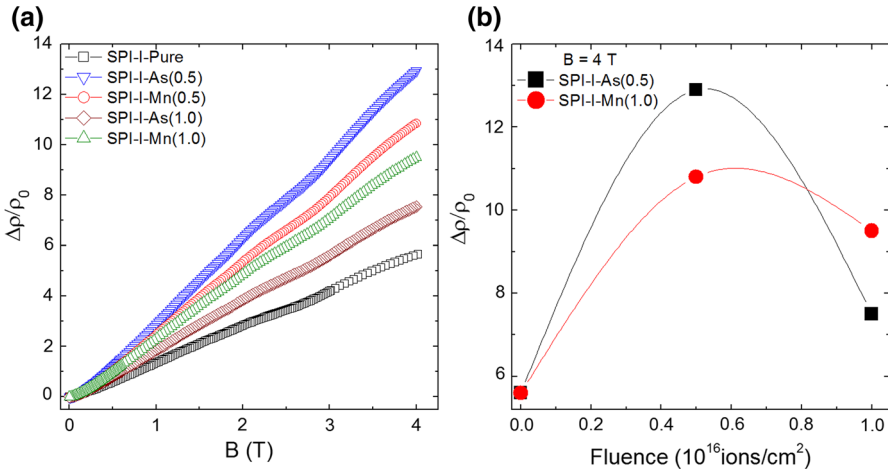
(a)

(b)

Fig. 5 **a** Planar magnetoresistance of pure SPI-I sample and irradiated with As and Mn as quoted. Measurements were carried out in the field interval $0 \leq B \leq 4T$ and fixed temperature $T = 2$ K. The average value of the longitudinal resistances at zero field for the measured samples is $R_{xx}(0) \approx 1.6\ \Omega$ at $T = 2$ K. **b** Magnetoresistance amplitude in $B = 4T$ as a function of the fluence (Color figure online)

produced by these defects somehow enhances the magnetoresistance. Considering that the magnetoresistance in graphite is related to the orbital motion of carriers instead of scattering, inhomogeneities play an important role in the transport properties when producing meandering of the electrical current. If the regions encircling vacancies in graphite become poorly conducting, an increase in the MR amplitude may be expected [46]. On the other hand, our Raman results indicate that higher fluences lead to a complete amorphization of the thin irradiated superficial layer. Amorphous carbon is well known to display very small MR [6]. As shown in data of Table 1, the penetration depth of the implanted ions amounts to 16 - 18 nm. This value is significantly smaller than the thickness of the layer probed by the electrical current, that we estimate to be about 100 nm when taking in account the contact configuration and the typical conductivity anisotropy of HOPG ($\sigma_c/\sigma_{ab} \approx 10^{-4}$[6]). Then, the superficial and amorphous layer conducts in parallel to less damaged deeper layers, leading to a decrease of the overall MR upon the subsequent augmentation of the fluence.

Shubnikov–de Haas oscillations may be observed superimposed to MR results in Fig. 5a. The relatively small magnitude of the SdH oscillations of SPI-I HOPG as compared to much stronger oscillations observed in graphite samples from other sources, such as ZYA or GW [18,36,46] was explained in terms of the relatively less pronounced surface roughness in SPI-I [36,47]. To extract the SdH oscillations from the results in Fig. 5a, the second derivative ($d^2 R_{xx}/dB^2$) was numerically calculated. This simple procedure allows removing from the raw data most of the regular field-dependent magnetoresistance. Typical $d^2 R_{xx}/dB^2$ results are shown in Fig. 6a.

The quantum fundamental frequencies $F = (\hbar/2\pi e)S_{\text{extr}}$, where S_{extr} is the extreme cross-sectional area of the Fermi surface and other symbols have the usual meaning [34], were obtained from the analysis of the $d^2 R_{xx}/dB^2$ data with a fast Fourier transform (FFT) software. The carrier effective masses were then calculated from the
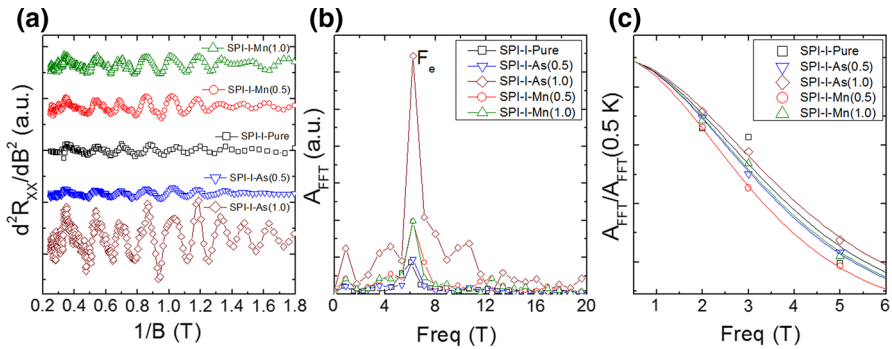
Fig. 6 **a** Representative $d^2 R_{xx}/dB^2$ data showing SdH oscillations for pure and implanted SPI-I graphite at $T = 2$ K as a function of the inverse of the induction. **b** Spectral intensity obtained from fast Fourier transform analysis of the data in panel (**a**). The F_e peak is identified to electron carriers. **c** Normalized amplitudes of the F_e peaks in panel (**b**) as functions of the temperature. Solid lines are fittings to the LK theory [34] (Color figure online)

temperature dependence of the normalized FFT amplitude (A_{FFT}) by using the thermal damping factor of the LK theory [34]. Due to the low SdH oscillation amplitudes, only the three lowest studied temperatures ($T = 2, 3, 5$ K) could be used for estimating A_{FFT}.

Figure 6a shows the SdH oscillations obtained from the second derivative of the longitudinal resistance at $T = 2$ K. Figure 6b shows the spectral density of the $d^2 R_{xx}/dB^2$ data obtained from fast Fourier transform. In all cases, the same quantum frequency was observed, indicating that implantation does not produce carrier doping in HOPG, as previously demonstrated [18]. Although graphite is a semimetal where hole and electron carriers should be present [8,9], only a single A_{FFT} peak corresponding to the electron pocket is visible in Fig. 6b [11–14]. This result suggests that transport by electron carriers is largely dominant in SPI-I HOPG, probably due to larger electron mobility. Data from Ref. [36] lead to the same conclusion. In Fig. 6c, fittings (colored lines) of the normalized FFT amplitudes versus temperature results to the LK theory [34] are shown for all studied samples. Though limited to the lowest measured temperatures, these fittings describe the experimental data fairly well and allow the estimation of the carrier effective masses. Since the observable FFT peak amplitude corresponds to electrons, only the effective masses for this type of carriers could be estimated from the LK theory. In Table 2, the values derived from our data for the fundamental frequencies and effective masses are listed. The obtained results are within the range of values reported for these parameters for pure HOPG [48]. Clearly, data in Table 2 do not hint to a doping effect produced by ion implantation in SPI-I HOPG. The obtained values rather point to impurity independent SdH fundamental frequencies and electron carrier effective masses. Though the average ion penetration depth is roughly a sixth part of the layer probed by the current, one might expect to observe systematic modifications of the SdH fundamental frequencies and/or the electron effective masses in the case of doping of graphite by the implanted ions. One must recognize, however, that the superficial layers mostly affected by the implantation are severely damaged and the carrier mean-free path become so small that the contribution of this region

Table 2 Fundamental frequencies and electron effective masses deduced from SdH oscillations in SPI-I-HOPG

Sample					
	SPI-I-Pure	SPI-I-As(0.5)	SPI-I-As(1.0)	SPI-I-Mn(0.5)	SPI-I-Mn(1.0)
Frequency	6.08	6.23	6.22	6.22	6.23
Effective mass	0.047 ± 0.013	0.049 ± 0.001	0.044 ± 0.002	0.054 ± 0.001	0.048 ± 0.003

of the sample to the SdH oscillations likely vanish. If the impurity concentration in the layers beyond the average ion penetration depth remains insufficient to produce doping effects, the SdH frequency and effective masses would not be modified. Nevertheless, we notice that implantation produces sizeable, but non-systematic, effects in the amplitude of the SdH oscillations, as shown in panel (a) of Fig. 6. In most cases these amplitudes are larger in the implanted samples, which is expected with basis on a resistivity enhancement due to disorder.

4 Conclusion

In this work, we have carried out Raman spectroscopy and electrical transport measurements in pure and ion-implanted HOPG graphite, grade SPI-I. Arsenide and manganese ions were implanted at low energy with two different fluences. The electrical transport experiments were performed with non-uniformly distributed current that flowed mostly near the irradiated HOPG surface. Raman experiments showed strong modifications upon the ion irradiation. For a fluence $\varphi = 0.5 \times 10^{16}/cm^2$, independently of the implanted ion, the amplitude of the G-peak is largely depressed due to the strong damage produced by irradiation. At this fluence, for both As and Mn implantation, the amplitude of the planar magnetoresistance increases and goes through a maximum, while the resistance versus temperature curves become flatter. For the highest studied fluence, $\varphi = 1.0 \times 10^{16}/cm^2$, the irradiated surface becomes completely amorphous, so that the G-peak is not observable in the Raman spectra. For this fluence, the magnitude of the MR becomes smaller, indicating that the amorphous carbon sheet near the HOPG surface conducts in parallel with deeper and less damaged graphene-type layers still probed by the current.

The study of the Shubnikov–de Haas oscillations in the MR allowed the determination of the quantum fundamental frequencies and the effective masses of the electron-type charge carriers. The obtained values are in accordance with those found in the literature for pure HOPG. This result implies that the implantation of As or Mn ions does not modify the carrier density of graphite. Effects related to the magnetic nature of the Mn impurities are not observed either. Consequently, the dominant effect produced by implantation in HOPG is the disorder in the atomic positions, independently of the irradiated ion. This disorder is particularly intense at the highest applied fluence, $\varphi = 1.0 \times 10^{16}/cm^2$, and leads to amorphization of the material in the superficial layer with thickness roughly corresponding to the ion penetration depth.

References

1. A.K. Geim, K.S. Novoselov, Nat. Mater. **6**, 183 (2007)
2. Y. Kopelevich, J.H.S. Torres, R.R. da Silva, F. Mrowka, H. Kempa, P. Esquinazi, Phys. Rev. Lett. **90**, 156402 (2003)
3. Y. Kopelevich, P. Esquinazi, Adv. Mater. **19**, 4559 (2007)
4. M. Inagaki, *New Carbons - Control of Structure and Functions* (Elsevier, Amsterdam, 2000)
5. J.D. Bernal, Proc. R. Soc. Lond. Ser. A **106**, 749 (1924)
6. D.D.L. Chung, J. Mater. Sci. **37**, 1475 (2002)
7. P. Wallace, Phys. Rev. **71**, 622 (1947)
8. J.C. Slonczewski, P.R. Weiss, Phys. Rev. **109**, 272 (1958)
9. J.W. McClure, Phys. Rev. **108**, 612 (1957)
10. P. Stamenova, V. Krsticb, J.M.D. Coey, J. Magn. Magn. Mater. **290–291**, 1402 (2005)
11. S.B. Hubbard, T.J. Kershaw, A. Usher, A.K. Savchenko, A. Shytov, Phys. Rev. B **83**, 035122 (2011)
12. W.J. Spry, P.M. Scherer, Phys. Rev. **120**, 826 (1960)
13. S.J. Williamson, S. Foner, M.S. Dresselhaus, Phys. Rev. A **140**, 1429 (1965)
14. R. Höhne, P. Esquinazi, V. Heera, H. Weishart, A. Setzer, D. Spemann, J. Magn. Magn. Mater. **320**, 966 (2008)
15. H. Xia, W. Li, Y. Song, X. Yang, X. Liu, M. Zhao, Y. Xia, C. Song, T.-W. Wang, D. Zhu, J. Gong, Z. Zhu, Adv. Mater. **20**, 4679 (2008)
16. X. Yang, H. Xia, X. Qin, W. Lia, Y. Daia, X. Liu, M. Zhao, Y. Xia, S. Yan, B. Wang, Carbon **47**, 1399 (2009)
17. R.F. Pires, P. Pureur, M. Behar, J.L. Pimentel Jr., J. Schaf, Y. Kopelevich, J. Appl. Phys. **111**, 093922 (2012)
18. R.F. de Jesus, B.C. Camargo, R.R. da Silva, Y. Kopelevich, M. Behar, M.A. Gusmão, P. Pureur, Phys. B **500**, 118 (2016)
19. M. S. Dresselhaus, *Solid State Physics* (Part I, Transport Properties of Solids, 2001)
20. P. Esquinazi, D. Spemann, R. Höhne, A. Setzer, K.-H. Han, T. Butz, Phys. Rev. Lett. **91**, 227201 (2003)
21. K.W. Lee, C.E. Lee, Phys. Rev. Lett. **97**, 137206 (2006)
22. Y. Wang, P. Pochet, C.A. Jenkins, E. Arenholz, G. Bukalis, S. Gemming, M. Helm, S. Zhou, Phys. Rev. B **90**, 214435 (2014)
23. M.S. Dresselhaus, A. Jorio, R. Saito, Ann. Rev. Condens. Matter. Phys. **1**, 89 (2010)
24. S.A. Soli, A.K. Ramdas, Phys. Rev. B **1**, 1687 (1970)
25. S. Prawer, R.J. Nemanich, Philos. Trans. R. Soc. Lond. A **362**, 2537 (2004)
26. N. Mounet, N. Marzari, Phys. Rev. B **71**, 205214 (2005)
27. J.-A. Yan, W.Y. Ruan, M.Y. Chou, Phys. Rev. B. **77**, 125401 (2008)
28. E.H. Martins Ferreira, M.V.O. Moutinho, F. Stavale, M.M. Lucchese, R.B. Capaz, C.A. Achete, A. Jorio, Phys. Rev. B **82**, 125429 (2010)
29. P. Tan, Y. Deng, Q. Zhao, Phys. Rev. B **58**, 5435 (1998)
30. A.F. Garcia-Flores, H. Terashita, E. Granado, Y. Kopelevich, Phys. Rev. B **79**, 113105 (2009)
31. B.S. Elman, M.S. Dresselhaus, G. Dresselhaus, E.W. Maby, H. Mazurek, Phys. Rev. B **24**, 1027 (1981)
32. J. Liu, M.D. Hou, C. Trautmann, R. Neumann, C. Müller, Z.G. Wang, Q.X. Zhang, Y.M. Sun, Y.F. Jin, H.W. Liu, H.J. Gao, Nucl. Instrum. Methods B **212**, 303 (2003)
33. H. Watanabe, K. Takahashi, M. Iwaki, Nucl. Instrum. Methods B **80**, 1489 (1993)
34. L.M. Lifshitz, M.A. Kosevich, Zh Eksp, Teor. Fiz. **29**, 730 (1955)
35. Z.-M. Wang, D.-Y. Xing, S.-Y. Zhang, Q.-Y. Xu, M. VanBael, Y.-W. Du, Chin. Phys. Lett. **24**, 199 (2007)
36. B.C. Camargo, Y. Kopelevich, A. Usher, S.B. Hubbard, App. Phys. Lett. **108**, 031604 (2016)
37. J.F. Ziegler, M.D. Ziegler, J.P. Biersack, Nucl. Instrum. Methods B **268**, 1818 (2010)
38. E. Koren, A.W. Knoll, E. Lörtscher, U. Duerig, Appl. Phys. Lett. **105**, 123112 (2014)
39. S. Reich, C. Thomsen, Philos. Trans. R. Soc. Lond. A **362**, 2271 (2004)
40. D. Graf, F. Molitor, K. Ensslin, C. Stampfer, A. Jungen, C. Hierold, L. Wirtz, Nano Lett. **7**, 238–242 (2006)
41. I.A. Luk'yanchuk, Y. Kopelevich, M. El Marssi, Phys. B **404**, 404 (2009)
42. M. Le Guillout, J.N. Rouzaud, D. Deldicque, N. Toulhoat, Y. Pipon, N. Moncoffre, Carbon **94**, 277 (2015)
43. B.T. Kelly, *Physics of Graphite* (Applied Science Publishers, London, 1981), p. 477

44. P. L. Walker Jr, P. A. Thrower, *Chemistry and Physics of Carbon* (Marcel Dekker, 1981)
45. M. Nastasi, J.W. Mayer, *Ions Implantation and Synthesis of Materials* (Springer, Berlin, 2006)
46. M.M. Parish, P.B. Littlewood, Nature **426**, 162 (2003)
47. B. C. Camargo, *Efeitos Quânticos em Semimetais de Dirac e Heteroestruturas Relacionadas*, Thesis – Instituto de Física Gleb Wataghin – Universidade Estadual de Campinas (UNICAMP), 2014
48. N.B. Brandt, S.M. Chudinov, Ya G. Ponomarev, *Semimetals I, Graphite and its Compounds* (Elsevier, Amsterdam, 1988)